Mechanical properties of high strength steels and weld metals at arctic low temperatures

Man-Tai Chen [a,b], Ao Cai [b], Madhup Pandey [c], Chen Shen [d], Yuelong Zhang [d], Lili Hu [a,b*]

[a] *State Key Laboratory of Ocean Engineering, Shanghai Jiao Tong University, Shanghai 200240, China*

[b] *Shanghai Key Laboratory for Digital Maintenance of Buildings and Infrastructure, Department of Civil Engineering, Shanghai Jiao Tong University, Shanghai 200240, China*

[c] *Department of Civil Engineering, University of Nottingham, UK*

[d] *Shanghai Key Lab of Materials Laser Processing and Modification, School of Materials Science and Engineering, Shanghai Jiao Tong University, Shanghai, 200240, China*

Abstract

This paper attempts to acquire fundamental knowledge on the mechanical properties of high strength steels and the corresponding high strength weld metals at arctic low temperatures. Two types of high strength steels (Q890, Q960) and three types of high strength weld metals (made of ER100S-G, ER110S-G, ER120S-G feedstock wires) were tested at arctic low and ambient temperatures ranging from -75°C to 25°C. Tensile coupon specimens for steel materials were directly extracted from high strength steel plates, whilst robotic gas metal arc welding was employed to fabricate the tensile specimens of weld metals. The tensile coupon specimens were designed as per ASTM E8M and wire-cut into shapes. Twenty-three tensile coupon tests on high strength steels and eighteen tensile coupon tests on high strength weld metals were carried out. Coupon specimens were tested in liquid nitrogen cooling chamber to mimic the arctic low temperature environment. The stress-strain responses and key mechanical properties of high strength steels and weld metals at both ambient and arctic low temperatures are presented and discussed. Prediction equations for key mechanical properties, including the Young's modulus, yield stress and ultimate tensile strength, of high strength steels and weld metals at arctic low temperatures were proposed.

Keywords: High strength steel; Low temperature; Mechanical properties; Tensile coupon tests; Weld metal.

---

* Corresponding author.
E-mail address: lilihu@sjtu.edu.cn (Lili Hu).

1. Introduction

Reducing carbon emission and reaching carbon neutrality are the urgent issues to be addressed in construction industry that need the joint efforts from different parties, such as research institutes, manufacturing industries, construction sectors and governments. To struggle toward carbon neutrality, researchers have sought to innovate the high performance construction materials [1-12] and structure systems [13-27] in order to improve the efficiency of engineering structures. In the meantime, the metallurgical industry has sought to develop advanced manufacturing technologies [28-31] and new steel tubular section profiles, e.g. round-ended oval [32, 33], semi-oval [34-37], polygonal [38-40] and elliptical sections [41-45], so as to offer various design alternatives for engineers. The use of high strength steel materials would facilitate in the reduction of self-weight of structures and associated handling, fabrication, transportation costs and erection time [46-50]. Therefore, high strength steel structures are favorable for both onshore and offshore engineering projects [51].

The engineering structures might suffer from different disasters during the lifecycle. Extensive research studies have been conducted on the performance of structures subjected to seismic attack [52-59], fire exposure [60-67], impact and blast loads in material, structural member and system levels. The low temperature environment could also be another disastrous situation for steel structures in arctic regions [68]. The structural design and operation of the arctic structures face immense challenges. It is crucial to understand the fundamental mechanical properties for the structural performance evaluation of the arctic structures. The low temperature mechanical properties of different types of normal strength steel have been conducted by various researchers [69-72]. Regarding high strength steel, Tong *et al.* [73] investigated the impact toughness properties and fracture mechanism of high strength structural steel with the nominal yield strength of 460, 690, 800 and 960 MPa as well as heat affected zone and weld metal at ambient and low temperatures (20°C to -40°C). Yan *et al.* [74] studied the stress-strain responses and tensile mechanical properties of Q690 and Q960 high strength structural steel at low temperatures ranging from -80 to 20°C. It was found that the tensile strength and ductility (in terms of fracture strain) of high strength steel materials

increased at low temperatures. Controversially, Azhari *et al.* [75] carried out tensile coupon tests on high strength steel at low temperatures of -40 and -80°C, and found that the tensile strength of high strength steel increased at low temperatures while the ductility decreased. In order to promote the future structural application of high strength steel structures in polar cold regions, it is important to acquire fundamental understanding on the mechanical properties of high strength steel and the corresponding weld metal materials. However, recent investigation on the low temperature behavior of high strength structural steel materials is very limited and that on high strength weld metals is even more scarce.

The present study attempts to unfold the lack of knowledge on the mechanical properties of high strength steels and the corresponding high strength weld metals at arctic low temperatures via experimental investigation. High strength steels with two steel grades (Q890, Q960) and three types of high strength weld metals (made of ER100S-G, ER110S-G, ER120S-G feedstock wires) were considered. Since it was recorded that the lowest temperature in the arctic regions can reach -72°C [76, 77], the temperatures ranging from 25°C (the ambient temperature) to -75°C were chosen for the tensile tests in this study. Twenty-three high strength steels and eighteen high strength weld metals tensile coupon specimens were tested at arctic low and ambient temperatures ranging from -75°C to 25°C. The stress-strain responses and key mechanical properties of high strength steels and weld metals at both ambient and arctic low temperatures were determined and discussed. Prediction equations for key mechanical properties, including the Young's modulus, yield stress and ultimate tensile strength, of high strength steels and weld metals at arctic low temperatures were proposed.

2. Details of test specimens

A series of uniaxial tensile tests were performed to derive the mechanical properties of high strength steels and weld metals at ambient and arctic low temperatures. Five temperatures were considered for each test series, namely 25°C, -20°C, -40°C, -60°C and -75°C (i.e. 298.15K, 253.15K, 233.15K, 213.15K and 198.15K in Kelvin temperature, respectively).

Flat tensile coupon specimens of high strength steels were extracted from heat-treated steel plates with two different steel grades (Q890, Q960) and two different thicknesses (t = 6mm, 8mm). The chemical compositions of each steel types provided in the corresponding mill certificates are shown in Table 1. The tensile coupon specimens at the ambient temperature were designed as per the American standard ASTM-E8M [78], whilst those at the low temperatures were specially designed so as to keep the dimensions of the parallel portion and to cater for the testing apparatus. A hole with diameter of 40 mm were made on each end with the 15 mm end clearance to mitigate net section failure near the holes for the low temperature coupon specimens. The dimensions of both ambient and low temperature coupon specimens are shown in Figs. 1a and 1b.

For high strength weld metals coupon specimens, three feedstock wires types of different grades (ER100S-G, ER110S-G, ER120S-G) with a diameter of 1.2 mm were used to fabricate the weld metal coupon specimens by robotic gas metal arc welding. The Fronius VR7000 welding machine and YASKAWA DX100 robotic arm were employed as shown in Fig. 2. The deposition current, voltage, and the travel speed were set as 165 A, 18 V, and 36 mm/min, respectively. Three weld chambers, one for each feedstock wire type, were fabricated to deposit filler material. The weld filler materials were deposited layer by layer along the trench until the chamber was fully filled. The dwelling time between successive layers was taken as 1 min. The weld metal tensile coupon specimens were then machined from the weld chamber with the longitudinal direction of coupon specimen perpendicular to the welding trench to replicate the welding and loading directions of butt-welded connections. A set of six (including one repeated test for each feedstock wire type) tensile coupon specimens to be tested at five different temperatures were extracted from the same weld chamber. The dimensions of high strength weld metal coupon specimen were designed as shown in Fig. 1c, which were in accordance with the American standard ASTM-E8M [78]. It should be noted that the region of reduced section, within which the specimen was expected to fail, was all made of weld metals.

Twenty-three high strength steel tensile coupon specimens and eighteen high strength weld

metal tensile coupon specimens were designed, fabricated and tested. In terms of the naming system of tensile coupon specimens, the first letter denotes the material types, where 'S', 'V' and 'W' mean Q960 super high strength steel, Q890 very high strength steel, and weld metal, respectively. The following number denotes the nominal thickness of the steel plate for high strength steel coupon and the feedstock wire type for weld metal coupon ('0', '1' and '2' mean ER100S-G, ER110S-G and ER120S-G, respectively). For coupon specimen at low temperature, a letter 'T' and a following number is used to denote the test temperature. The letter 'R' is used to denote the repeated test.

3. Tensile test instrumentation and operation

The coupon specimens were tested at 25°C (ambient temperature), -20°C, -40°C, -60°C and -75°C using the steady-state test method in the 500kN MTS machine. The tensile test instrumentations of coupon tests for high-strength steels and weld metals at ambient and low temperatures were different as shown in Fig. 3. The high strength steel specimens at ambient temperature were installed by gripping both ends with flat surface clamps in the test rig (Fig. 3a), whilst the high strength steel specimens at low temperature were installed between two pins in the loading rigs (Fig. 3b). The high strength weld metal specimens at both ambient and low temperatures were installed by fixing both ends into the test rigs with screw threads (Fig. 3b).

For tensile tests at low temperatures, liquid nitrogen as the cryogen and an environmental chamber with a temperature control unit were used in this study to create the low temperature environment. After careful installation and alignment of specimen in the test rig, the cooling chamber was closed and liquid nitrogen was then injected into the chamber to cool down the environment and the specimen. Thermocouples were installed in the chamber as well as on the specimen surface at the reduced section so as to monitor the temperatures of the test environment and the specimen surface. The liquid nitrogen inflow was discretely controlled with reference to the thermocouples' readings in the chamber to avoid the over cooling of the specimen and to stabilize the specimen surface temperature when the target temperature was reached. The soaking time of 10 mins prior to the formal

tensile test was incorporated to facilitate the uniform temperature distribution of steel coupon specimen.

The real-time longitudinal strains of high strength steel and weld metal coupon specimens were instrumented by the MTS model 634.25F-24 and Epsilon model 3542-025M-025-LHT extensometers with 50 mm and 25 mm gauge lengths, respectively. The allowable temperature ranges for the MTS and Epsilon extensometers are -85°C to 120°C and -270°C to 200°C, respectively. The uniaxial tension was applied using a displacement-controlled mode at the rates of 0.1 and 0.5 mm/min for elastic and plastic ranges, respectively. The loading rate of 0.5mm/min for plastic range fell within the recommended range of loading rates by Huang and Young [79]. Slower loading rate of 0.1mm/min was employed for elastic range such that more data could be recorded to derive the Young's modulus of steel material. The applied displacement was halted for 100 s near yield stress and ultimate load to allow for stress relaxation and to derive the static stress-strain response, as previously adopted in Ref. [80-85]. The tensile specimens were loaded to fracture. The applied tension as well as the readings of extensometer were logged at regular intervals throughout the tensile coupon tests.

4. Tensile test results and discussions

4.1. Stress-strain responses and failure patterns

The measured static stress-strain responses of the high strength steels and weld metals at various temperature exposures are shown in Figs. 4 and 5, respectively. The stress-strain responses for high strength steel plates with different thicknesses were similar. The overall shapes of the stress-strain curves for specimens at low temperatures were similar to the counterpart at ambient temperature, except that certain extent of tensile behavior improvement was observed from the perspectives of both strength and ductility. The quantitative improvements on the mechanical properties due to the low temperature effect are discussed in the following sections.

The failure patterns of the high strength steels and weld metals at various temperatures are

shown in Fig. 6. No brittle failure was observed, even for those specimens tested at low temperatures. All the 23 high strength steel coupon specimens and 18 high strength weld metal coupon specimens exhibited ductile failure, evident by the occurrence of necking at the reduced section prior to fracture.

The mechanical properties of coupon specimens were obtained from static stress-strain responses. Table 2 shows the mechanical properties of coupon specimens at ambient temperature, including the Young's modulus (E), yield stress ($\sigma_{0.2}$), ultimate strength (σ_u) and fracture strain (ε_f). The mechanical properties of high strength steels and weld metals at low temperatures are tabulated in Tables 3 and 4, respectively, where an additional subscript 'T' was used to denote the corresponding low temperature mechanical property. It was found that the differences between the results obtained from the first and respective repeated tests were small, indicating the reliability of test results. The retention factors defined by the ratio of mechanical properties at low temperatures to ambient temperature are also reported in Tables 3 and 4 in order to investigate the effect of low temperature.

4.2. Young's modulus

The retention factor of the Young's modulus (k_E=E_T/E) was employed to investigate the influence of low temperature on Young's modulus. The values of k_E for high strength steels and weld metals are tabulated in Tables 3 and 4, respectively. The values of k_E for Q890 and Q960 high strength steels obtained from this study ranged from 1.04 to 1.10 and 1.02 to 1.12, respectively. Whilst the retention factor of the Young's modulus for weld metal coupons made of ER100S-G, ER110S-G and ER120S-G feedstock wires ranged from 1.01 to 1.06, 1.00 to 1.05 and 0.98 to 1.04, respectively. The retention factor of the Young's modulus (k_E) is plotted against the test specimen temperature in Figs. 7a and 7b for high strength steels and weld metals, respectively. In general, the low temperature somehow led to the increase in the Young's modulus for both high strength steels and weld metals as evident by the values of k_E greater than unity. The low temperature effect was relatively more significant for high strength steels.

4.3. Yield stress and ultimate tensile strength

It can be observed from Figs. 4 and 5 that the stress-strain curves of high strength steels and weld metals at both ambient and low temperatures did not exhibit the sharp-kneed shape with distinct yield plateau. Therefore, the 0.2% offset method was adopted to derive the yield stress of high strength steels and weld metals. The values of the retention factors of yield stress ($k_{0.2}=\sigma_{0.2T}/\sigma_{0.2}$) and ultimate tensile strength ($k_u=\sigma_{uT}/\sigma_u$) for Q890 and Q960 high strength steels are tabulated in Table 3, and those for weld metal coupon specimens made of ER100S-G, ER110S-G and ER120S-G feedstock wires are tabulated in Table 4. The retention factors of yield stress ($k_{0.2}$) and ultimate tensile strength (k_u) are plotted against the test specimen temperature in Figs. 8a and 8b for high strength steels and weld metals, respectively.

It was found that both the yield stress and ultimate tensile strength increased when the specimen temperature decreased for Q890 and Q960 high strength steels. The trend of yield stress and ultimate tensile strength increments with low temperature was apparent, implying high correlation between $\sigma_{0.2T}$ and low temperature as well as between σ_{uT} and low temperature for Q890 and Q960 high strength steels. When the temperature reduced from 25°C to -75°C, the increase in yield stress could reach 9% and 10% for Q890 and Q960 high strength steels, respectively, whilst the ultimate tensile strength was increased by 10% and 9% for Q890 and Q960 high strength steels, respectively.

The yield stress and ultimate tensile strength also increased with the reduction in specimen temperature for ER100S-G, ER110S-G and ER120S-G high strength weld metals. However, the low temperature influence on the yield stress was less significant, whilst the low temperature influence on the ultimate tensile strength was more significant for high strength weld metals compared to those for high strength steels. The trend of yield stress and ultimate tensile strength increments with low temperature was also apparent for ER100S-G, ER110S-G and ER120S-G high strength weld metals. When the temperature reduced from 25°C to -75°C, for ER100S-G, ER110S-G and ER120S-G weld metals, the increases of yield stress were 4%, 6% and 5%, respectively, whilst the ultimate tensile strength was increased by 14%, 11% and 12%, respectively. Such improvements in the yield stress

and ultimate tensile strength of high strength steels and weld metals were attributed to the more compact microstructure and larger molecular force of metallic specimens at arctic low temperatures [74].

4.4. Strain at fracture

The values of the retention factor of the strain at fracture (k_f=ε_{fT}/ε_f) for high strength steels and weld metals are tabulated in Tables 3 and 4, respectively. The values of k_f for Q890 and Q960 high strength steels ranged from 1.09 to 1.35 and 0.99 to 1.33, respectively. Whilst the values of k_f for weld metal coupons made of ER100S-G, ER110S-G and ER120S-G feedstock wires ranged from 1.04 to 1.22, 1.07 to 1.23 and 1.02 to 1.16, respectively. The low temperature generally led to the increase in the strain at fracture for both high strength steels and weld metals as evident by the values of ε_{fT}/ε_f greater than unity. Similar finding was reported by Yan *et al.* [74] for high strength steels. The low temperature effect was relatively more significant for high strength steels. However, the trend of fracture strain increment with temperature was not apparent.

5. Proposed prediction equations for mechanical properties at low temperatures

5.1. General

The retention factors were employed to predict the mechanical properties of high strength steels at low temperatures. The unified equation in exponential format for steel materials at low temperatures previously adopted by Yan *et al.* [74, 77] was employed in this study. It was stated that the effect of thickness could be ignored if the chemical compositions for steel plates with different thicknesses varying from 3 to 12 mm are similar [74, 77]. Therefore, the critical parameters affecting the low temperature mechanical properties were the mechanical properties at ambient temperature (X) and low temperature (T). In this study, the unified equation was simplified accordingly as shown in Eq. (1).

$$k_{X,P} = \frac{X_{T,P}}{X} = aT^b X^c \quad (1)$$

where $k_{X,P}$ is the retention factor for a particular mechanical property X, including the Young's modulus E, yield stress $\sigma_{0.2}$ and ultimate tensile strength σ_u. T denotes the specimen temperature in Kelvin degree. $X_{T,P}$ and X are the values of predicted mechanical properties at low temperature and mechanical properties at ambient temperature 298.15K (25°C), respectively. The coefficients a, b and c were calibrated with the existing data of low temperature mechanical properties by the best subset regression analysis. By taking logarithm on both sides of Eq. (1), simplified linear relationship can be yielded as shown in Eq. (2) for further regression analysis.

$$\ln k_{X,P} = \ln a + b\ln T + c\ln X \tag{2}$$

5.2. High strength steels at low temperatures

The low temperature mechanical properties of high strength structural steels derived in this study as well as those reported by Yan *et al.* [74] were used to propose the equations describing the low temperature retention factors. The best subset regression analysis was adopted to select the most critical predictors and determine the corresponding coefficients in the prediction equation. Table 5 lists all three possible predictor subsets in the prediction equation for each mechanical property. The coefficient of determination (R^2) and Mallows Cp index are important indicators to examine the predicting capacity of the model. The predictor subset with the coefficient of determination (R^2) closer to unity and smaller Cp value is preferred. In addition, the number of predictors is also an important indicator for the simplicity of prediction model and should be also considered. Results of the best subset regression analyses for high strength steel low temperature mechanical properties predictions are shown in Table 5. Model 1 with only one predictor of temperature (T) was selected for the retention factor predictions of Young's modulus, yield stress and ultimate tensile strength. The recommended prediction equations for high strength steel low temperature retention factor of Young's modulus, yield stress and ultimate tensile strength are shown in Eqs. (3)-(5), respectively.

$$k_{E,P} = \frac{E_{T,P}}{E} = 3.153T^{-0.201} \tag{3}$$

$$k_{0.2,P} = \frac{\sigma_{0.2T,P}}{\sigma_{0.2}} = 4.686T^{-0.271} \quad (4)$$

$$k_{u,P} = \frac{\sigma_{uT,P}}{\sigma_{u}} = 4.732T^{-0.273} \quad (5)$$

where T is the high strength steel specimen temperature in Kelvin degree and 193.15K$\leqslant T\leqslant$298.15K.

The comparisons between test and predicted low temperature retention factors of various mechanical properties, i.e. the Young's modulus, yield stress, ultimate tensile strength, are depicted in Fig. 10 and Table 3. The mean values of test-to-predicted Young's modulus ($E_T/E_{T,P}$), yield stress ($\sigma_{0.2T}/\sigma_{0.2T,P}$) and ultimate tensile strength ($\sigma_{uT}/\sigma_{uT,P}$) are equal to 1.005, 0.992 and 0.992 with the coefficient of variation (COV) being 0.046, 0.019 and 0.023, respectively, as shown in Table 3. Fig. 10 plots the predicted low retention factor against the corresponding test retention factor of various mechanical properties. It can be observed that almost all data points regarding the Young's modulus and all data points regarding the yield stress and ultimate tensile strength fall in the region with ±10% error. The results demonstrated that the proposed equations can accurately predict the low temperature mechanical properties of high strength steels with nominal yield stress ranged from 690 to 960 MPa exposed to the arctic low temperature ranging from 25°C (298.15K) to -80°C (193.15K).

5.3. High strength weld metals at low temperatures

The low temperature mechanical properties of high strength weld metals derived in this study were adopted to propose the equations describing the low temperature retention factors. The best subset regression analysis was adopted to derive the low temperature retention factor prediction equations for various mechanical properties, where details have been described in previous section. Results of the best subset regression analyses for high strength weld metal low temperature mechanical properties predictions are shown in Table 6. Model 1 with only one predictor of temperature (T) was selected for the retention factor predictions of Young's modulus, yield stress and ultimate tensile strength. The recommended prediction equations for high strength weld metal low temperature retention factor of Young's modulus, yield stress and ultimate tensile strength are shown

in Eqs. (6)-(8), respectively.

$$k_{E,P} = \frac{E_{T,P}}{E} = 2.068T^{-0.13} \quad (6)$$

$$k_{0.2,P} = \frac{\sigma_{0.2T,P}}{\sigma_{0.2}} = 1.856T^{-0.109} \quad (7)$$

$$k_{u,P} = \frac{\sigma_{uT,P}}{\sigma_u} = 4.757T^{-0.273} \quad (8)$$

where T is the high strength weld metal specimen temperature in Kelvin degree and 198.15K$\leqslant T\leqslant$ 298.15K.

The comparisons between test and predicted low temperature retention factors of various mechanical properties for high strength weld metals are depicted in Fig. 11 and Table 4. The mean values of test-to-predicted Young's modulus ($E_T/E_{T,P}$), yield stress ($\sigma_{0.2T}/\sigma_{0.2T,P}$) and ultimate tensile strength ($\sigma_{uT}/\sigma_{uT,P}$) are equal to 0.999, 1.001 and 1.001 with the coefficient of variation (COV) being 0.018, 0.014 and 0.010, respectively, as shown in Table 4. Fig. 11 plots the predicted low retention factor against the corresponding test retention factor of various mechanical properties. It can be observed that all data points fall in the region with ±5% error. The results demonstrated that the proposed equations can accurately predict the low temperature mechanical properties of high strength weld metals made of ER100S-G, ER110S-G, ER120S-G feedstock wires exposed to the arctic low temperature ranging from 25°C (298.15K) to -75°C (198.15K).

6. Concluding remarks

The tensile mechanical properties of high strength steels and weld metals at ambient and arctic low temperatures ranging from 25°C to -75°C were studied. Twenty-three tensile coupon tests on Q890 and Q960 high strength steels as well as eighteen tensile coupon tests on high strength weld metals made of ER100S-G, ER110S-G, ER120S-G feedstock wires were carried out. Based on the findings in this study, the following conclusions can be drawn.

(1) The Young's modulus, yield stress and ultimate tensile strength of high strength steels and weld metal generally increased with the decrease of arctic low temperature in relatively clear trend.

Although the trend of fracture strain increment with temperature was not apparent, the arctic low temperature did not reduce the ductility of high strength steels and weld metals.

(2) When the temperature reduced from 25°C to -75°C, the increase in the Young's modulus, yield stress and ultimate tensile strength for high strength steels could reach 12%, 10% and 10%, respectively. Whilst the increase in the Young's modulus, yield stress and ultimate tensile strength for high strength weld metals could reach 6%, 6% and 14%, respectively.

(3) Prediction equations for retention factors of the Young's modulus, yield stress and ultimate tensile strength of high strength steels and weld metals at arctic low temperatures were proposed based on the test results obtained from this study and the literature using the best subset regression analysis.

(4) The proposed equations can accurately predict the low temperature retention factors (and hence the low temperature mechanical properties) of high strength steels with nominal yield stresses ranged from 690 to 960 MPa exposed to the arctic low temperature ranging from 25°C to -80°C as well as high strength weld metals made of ER100S-G, ER110S-G, ER120S-G feedstock wires exposed to the arctic low temperature ranging from 25°C to -75°C.

Acknowledgements

The authors would also like to thank the support from the National Natural Science Foundation of China (No. 52108157), the Shanghai Sailing Program, China (No. 20YF1419400), and the Natural Science Foundation of Shanghai, China (No. 21ZR1429000).

Data Availability Statement

All data, models, and code generated or used during the study are available upon reasonable request.

References

[1] Lai M, Hanzic L, Ho JCM. Fillers to improve passing ability of concrete. Structural Concrete 2019;20(1):185-197.

[2] Lai MH, Binhowimal SAM, Hanzic L, Wang Q, Ho JCM. Dilatancy mitigation of cement powder paste by pozzolanic and inert fillers. Structural Concrete 2020;21(3):1164-1180.

[3] Zhong Y, Zhao O, Gardner L. Experimental and numerical investigation of S700 high strength steel CHS beam–columns after exposure to fire. Thin-Walled Structures 2022;175:109248.

[4] Zhong Y, Zhao O. Experimental and numerical studies on post-fire behaviour of S700 high strength steel circular hollow sections under combined compression and bending. Thin-Walled Structures 2022;181:110004.

[5] Zhong Y, Sun Y, Zhao O, Gardner L. Structural Response and Residual Capacity of S700 High-Strength Steel CHS Columns after Exposure to Elevated Temperatures. Journal of Structural Engineering 2022;148(6):04022050.

[6] Zhou Z, Ke K, Chen Y, Yam MCH. High strength steel frames with curved knee braces: Performance-based damage-control design framework. Journal of Constructional Steel Research 2022;196:107392.

[7] Lai MH, Zou J, Yao B, Ho JCM, Zhuang X, Wang Q. Improving mechanical behavior and microstructure of concrete by using BOF steel slag aggregate. Construction and Building Materials 2021;277:122269.

[8] Lai M, Wu K, Ou X, Zeng M, Li C, Ho JCM. Effect of concrete wet packing density on the uni-axial strength of manufactured sand CFST columns. Structural Concrete 2022;23:2615-2629.

[9] Ke K, Xiong YH, Yam MCH, Lam ACC, Chung KF. Shear lag effect on ultimate tensile capacity of high strength steel angles. Journal of Constructional Steel Research 2018;145:300-314.

[10] Lai MH, Chen ZH, Wang YH, Ho JCM. Effect of fillers on the mechanical properties and durability of steel slag concrete. Construction and Building Materials 2022;335:127495.

[11] Lai MH, Wu KJ, Cheng X, Ho JCM, Wu JP, Chen JH, Zhang AJ. Effect of fillers on the behaviour of heavy-weight concrete made by iron sand. Construction and Building Materials 2022;332:127357.

[12] Lai MH, Lao WC, Tang WK, Hanzic L, Wang Q, Ho JCM. Dilatancy swerve in superplasticized cement powder paste. Construction and Building Materials 2023;362:129524.

[13] Cheng B, Huang F, Duan Y, Chen MT. Fatigue Performance of Bird-Beak SHS Gap K-Joints under Brace In-Plane Force. Journal of Structural Engineering 2021;147(11):04021167.

[14] Ke K, Zhou X, Zhang H, Yam MCH, Guo L, Chen Y. Performance-based-plastic-design of damage-control steel MRFs equipped with self-centring energy dissipation bays. Journal of Constructional Steel Research 2022;192:107230.

[15] He X, Chen Y, Ke K, Shao T, Yam MCH. Development of a connection equipped with fuse angles for steel moment resisting frames. Engineering Structures 2022;265:114503.

[16] Zhou X, Zhang H, Ke K, Guo L, Yam MCH. Damage-control steel frames equipped with SMA connections and ductile links subjected to near-field earthquake motions: A spectral energy factor model. Engineering Structures 2021;239:112301.

[17] Zhou X, Ke K, Yam MCH, Zhao Q, Huang Y, Di J. Shape memory alloy plates: Cyclic tension-release performance, seismic applications in beam-to-column connections and a structural seismic demand perspective. Thin-Walled Structures 2021;167:108158.

[18] Lai MH, Li CW, Ho JCM, Chen MT. Experimental investigation on hollow-steel-tube columns with external confinements. Journal of Constructional Steel Research 2020;166:105865.

[19] Pandey M, Young B. Ultimate resistances of member-rotated cold-formed high strength steel

tubular T-joints under compression loads. Engineering Structures 2021;244:112601.
[20] Pandey M, Young B. Effect of member orientation on static strengths of cold-formed high strength steel tubular X-joints. Thin-Walled Structures 2022;170:108501.
[21] Ke K, Chen Y, Zhou X, Yam MC, Hu S. Experimental and numerical study of a brace-type hybrid damper with steel slit plates enhanced by friction mechanism. Thin-Walled Structures 2023;182:110249.
[22] Zhou X, Tan Y, Ke K, Yam MC, Zhang H, Xu J. An experimental and numerical study of brace-type long double C-section steel slit dampers. Journal of Building Engineering 2022:105555.
[23] Wang L, Zhang YW, Ho JCM, Lai MH. Fatigue behaviour of composite sandwich beams strengthened with GFRP stiffeners. Engineering Structures 2020;214:110596.
[24] Ho JCM, Ou XL, Li CW, Song W, Wang Q, Lai MH. Uni-axial behaviour of expansive CFST and DSCFST stub columns. Engineering Structures 2021;237:112193.
[25] Chen MT, Young B, Martins AD, Camotim D, Dinis PB. Experimental investigation on cold-formed steel lipped channel beams affected by local-distortional interaction under non-uniform bending. Thin-Walled Structures 2021;161:107494.
[26] Lai MH, Chen MT, Ren FM, Ho JCM. Uni-axial behaviour of externally confined UHSCFST columns. Thin-Walled Structures 2019;142:19-36.
[27] Ho JCM, Ou XL, Chen MT, Wang Q, Lai MH. A path dependent constitutive model for CFFT column. Engineering Structures 2020;210:110367.
[28] Wang L, Sun J, Ding T, Liang Y, Ho JCM, Lai MH. Manufacture and behaviour of innovative 3D printed auxetic composite panels subjected to low-velocity impact load. Structures 2022;38:910-933.
[29] Yan JJ, Chen MT, Quach WM, Yan M, Young B. Mechanical properties and cross-sectional behavior of additive manufactured high strength steel tubular sections. Thin-walled Structures 2019;144:106158.
[30] Xiao J, Ji G, Zhang Y, Ma G, Mechtcherine V, Pan J, Wang L, Ding T, Duan Z, Du S. Large-scale 3D printing concrete technology: Current status and future opportunities. Cement and Concrete Composites 2021;122:104115.
[31] Buchanan C, Gardner L. Metal 3D printing in construction: A review of methods, research, applications, opportunities and challenges. Engineering Structures 2019;180:332-348.
[32] Zhu JH, Young B. Cold-formed-steel oval hollow sections under axial compression. Journal of Structural Engineering 2011;137(7):719-727.
[33] Shen Q, Wang J, Liew JR, Gao B, Xiao Q. Experimental study and strength evaluation of axially loaded welded tubular joints with round-ended oval hollow sections. Thin-Walled Structures 2020;154:106846.
[34] Chen MT, Young B. Tests of cold-formed steel semi-oval hollow section members under eccentric axial load. Journal of Structural Engineering 2020;146(4):04020027.
[35] Chen MT, Young B. Beam-column design of cold-formed steel semi-oval hollow non-slender sections. Thin-Walled Structures 2021;162:107376.
[36] Chen MT, Zuo W, Young B. Tests of cold-formed steel T-joints with semi-oval hollow section chords. Journal of Structural Engineering 2023: (Submitted).
[37] Yi S, Chen MT, Young B. Stub column behavior of concrete-filled cold-formed steel semi-oval sections. Journal of Structural Engineering 2023: DOI: 10.1061/JSENDH/STENG-11667.
[38] Fang H, Chan TM, Young B. Material properties and residual stresses of octagonal high strength steel hollow sections. Journal of Constructional Steel Research 2018;148:479-490.
[39] Zhu JY, Chan TM, Young B. Cross-sectional capacity of octagonal tubular steel stub columns under uniaxial compression. Engineering Structures 2019;184:480-494.
[40] Ding FX, Li Z, Cheng S, Yu ZW. Composite action of hexagonal concrete-filled steel tubular stub columns under axial loading. Thin-Walled Structures 2016;107:502-513.

[41] Chen MT, Young B. Numerical analysis and design of cold-formed steel elliptical hollow sections under combined compression and bending. Engineering Structures 2021;241:112417.
[42] Chen MT, Young B. Beam-column tests of cold-formed steel elliptical hollow sections. Engineering Structures 2020;210:109911.
[43] Chen MT, Chen Y, Young B. Static strengths of cold-formed steel elliptical hollow section X-joints. Thin-Walled Structures 2023: (Submitted).
[44] Chen MT, Chen Y, Young B. Experimental investigation on cold-formed steel elliptical T-joints. Engineering Structures 2023: (Submitted).
[45] Yi S, Chen MT, Young B. Design of concrete-filled cold-formed steel elliptical stub columns. Engineering Structures 2023: DOI: 10.1016/j.engstruct.2022.115269.
[46] Jiang B, Yam MCH, Ke K, Lam ACC, Zhao Q. Block shear failure of S275 and S690 steel angles with single-line bolted connections. Journal of Constructional Steel Research 2020;170:106068.
[47] Ke K, Zhang M, Yam MCH, Lam ACC, Wang J, Jiang B. Block shear performance of double-line bolted S690 steel angles under uniaxial tension. Thin-Walled Structures 2022;171:108668.
[48] Lin X-M, Yam MC, Ke K, He Q, Chung K-F. Investigation of block shear strength of high strength steel bolted connections. Journal of Constructional Steel Research 2022;196:107407.
[49] Yam MCH, Ke K, Jiang B, Lam ACC. Net section resistance of bolted S690 steel angles subjected to tension. Thin-Walled Structures 2020;151:106722.
[50] Pandey M, Young B. Compression capacities of cold-formed high strength steel tubular T-joints. Journal of Constructional Steel Research 2019;162:105650.
[51] Pandey M, Young B. Structural performance of cold-formed high strength steel tubular X-Joints under brace axial compression. Engineering Structures 2020;208:109768.
[52] Zhang H, Zhou X, Ke K, Yam MC, He X, Li H. Self-centring hybrid-steel-frames employing energy dissipation sequences: Insights and inelastic seismic demand model. Journal of Building Engineering 2023;63:105451.
[53] Guan M, Liu W, Lai M, Du H, Cui J, Gan Y. Seismic behaviour of innovative composite walls with high-strength manufactured sand concrete. Engineering Structures 2019;195:182-199.
[54] Ren FM, Tian SY, Gong L, Wu JL, Mo JX, Lai CL, Lai MH. Seismic performance of a ring beam joint connecting FTCES column and RC/ESRC beam with NSC. Journal of Building Engineering 2023;63:105366.
[55] Ke K, Zhou X, Zhu M, Yam MCH, Wang Y, Zhang H. Seismic evaluation of industrial steel moment resisting frames with shape memory alloys using performance-spectra-based method. Journal of Building Engineering 2022;48:103950.
[56] Bian J, Zhou X, Ke K, Yam MCH, Wang Y. Seismic resilient steel substation with BI-TMDI: A theoretical model for optimal design. Journal of Constructional Steel Research 2022;192:107233.
[57] Chen Y, Ke K. Seismic performance of high-strength-steel frame equipped with sacrificial beams of non-compact sections in energy dissipation bays. Thin-Walled Structures 2019;139:169-185.
[58] Ke K, Chen Y. Seismic performance of MRFs with high strength steel main frames and EDBs. Journal of Constructional Steel Research 2016;126:214-228.
[59] Ke K, Yam MCH, Zhou X, Wang F, Xu F. Energy factor of high-strength-steel frames with energy dissipation bays under repeated near-field earthquakes. Steel and Composite Structures, An International Journal 2021;40(3):369-387.
[60] Su A, Sun Y, Liang Y, Zhao O. Material properties and membrane residual stresses of S690 high strength steel welded I-sections after exposure to elevated temperatures. Thin-Walled Structures 2020;152:106723.
[61] Su A, Jiang K, Liang Y, Zhao O. Post-fire behaviour and resistances of S690 high strength steel welded I-section stub columns. Thin-Walled Structures 2021;169:108422.

[62] Su A, Jiang K, Wang Y, Zhao O. Experimental and numerical investigations into S960 ultra-high strength steel welded I-section stub columns after exposure to elevated temperatures. Thin-Walled Structures 2023;183:110349.
[63] Zhong Y, Tan KH, Zhao O. Experimental and numerical investigations of S700 high strength steel tubular section stub columns after exposure to elevated temperatures. Thin-Walled Structures 2021;163:107669.
[64] Qiang X, Shu Y, Jiang X. Mechanical behaviour of high strength steel T-stubs at elevated temperatures: Experimental study. Thin-Walled Structures 2023;182:110314.
[65] Zhuang X, Liang Y, Ho JCM, Wang YH, Lai MH, Li XY, Xu ZH, Xu YN. Post-fire behaviour of steel slag fine aggregate concrete. Structural Concrete 2022;https://doi.org/10.1002/suco.202100677.
[66] Ho JCM, Liang Y, Wang YH, Lai M, Huang ZC, Yang D, Zhang QL. Residual properties of steel slag coarse aggregate concrete after exposure to elevated temperatures. Construction and Building Materials 2022;316:125751.
[67] Lai MH, Huang ZC, Wang CT, Wang YH, Chen LJ, Ho JCM. Effect of fillers on the behaviour of low carbon footprint concrete at and after exposure to elevated temperatures. Journal of Building Engineering 2022;51:104117.
[68] Hu L, Li M, Yiliyaer T, Gao W, Wang H. Strengthening of cracked DH36 steel plates by CFRP sheets under fatigue loading at low temperatures. Ocean Engineering 2022;243:110203.
[69] Rokilan M, Mahendran M. Sub-zero temperature mechanical properties of cold-rolled steel sheets. Thin-walled Structures 2020;154:106842.
[70] Tomita Y. Low temperature mechanical properties of modified heat treated 300M steel. Materials science and technology 1995;11(4):335-340.
[71] Holmen JK, Thomesen S, Perez-Martin MJ, Hopperstad OS, Børvik T. Ballistic impact of structural steels at low temperatures. Journal of Applied Mechanics 2022;89(10):101001.
[72] Yan J-B, Dong X, Zhu J-S. Behaviours of stub steel tubular columns subjected to axial compression at low temperatures. Construction and Building Materials 2019;228:116788.
[73] Tong L, Niu L, Jing S, Ai L, Zhao X-L. Low temperature impact toughness of high strength structural steel. Thin-Walled Structures 2018;132:410-420.
[74] Yan J-B, Luo Y-L, Lin X, Luo Y-B, Zhang L. Effects of the Arctic low temperature on mechanical properties of Q690 and Q960 high-strength steels. Construction and Building Materials 2021;300:124022.
[75] Azhari F, Apon A-AH, Heidarpour A, Zhao X-L, Hutchinson CR. Mechanical response of ultra-high strength (Grade 1200) steel under extreme cooling conditions. Construction and Building Materials 2018;175:790-803.
[76] Stepanova NA. On the lowest temperatures on earth. Monthly weather review 1958;86(1):6-10.
[77] Yan J-B, Liew JR, Zhang M-H, Wang J-Y. Mechanical properties of normal strength mild steel and high strength steel S690 in low temperature relevant to Arctic environment. Materials & Design 2014;61:150-159.
[78] ASTM E8M-16. Standard Test Methods for Tension Testing of Metallic Materials. West Conshohocken, PA, USA: ASTM; 2016.
[79] Huang Y, Young B. The art of coupon tests. Journal of Constructional Steel Research 2014;96:159-175.
[80] Chen MT, Young B. Tensile tests of cold-formed stainless steel tubes. Journal of Structural Engineering 2020;146(9):04020165.
[81] Chen MT, Young B. Tests of cold-formed normal and high strength steel tubes under tension. Thin-Walled Structures 2020;153:106844.
[82] Chen MT, Young B, Martins AD, Camotim D, Dinis PB. Experimental investigation on cold-formed steel stiffened lipped channel columns undergoing local-distortional interaction. Thin-Walled Structures 2020;150:106682.

[83] Chen MT, Young B, Martins AD, Camotim D, Dinis PB. Uniformly bent CFS lipped channel beams experiencing local-distortional interaction: Experimental investigation. Journal of Constructional Steel Research 2020;170:106098.
[84] Chen MT, Pandey M, Young B. Post-fire residual material properties of cold-formed steel elliptical hollow sections. Journal of Constructional Steel Research 2021;183:106723.
[85] Chen MT, Pandey M, Young B. Mechanical properties of cold-formed steel semi-oval hollow sections after exposure to ISO-834 fire. Thin-Walled Structures 2021;167:108202.

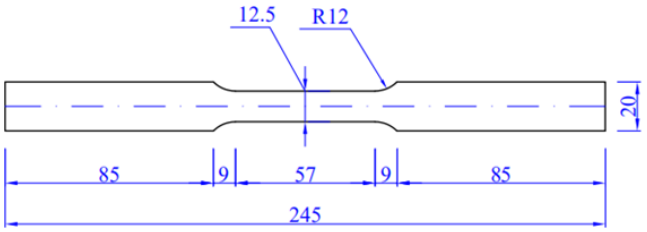

(a) Ambient temperature coupon

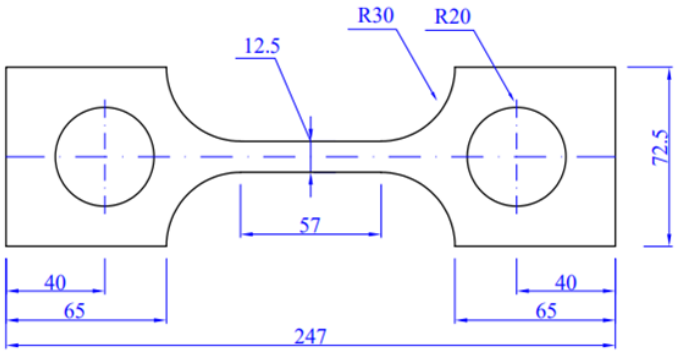

(b) Low temperature coupon

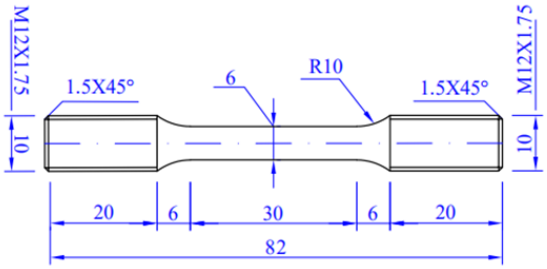

(c) Weld metal coupon

Fig. 1. Dimensions of tensile coupon specimens

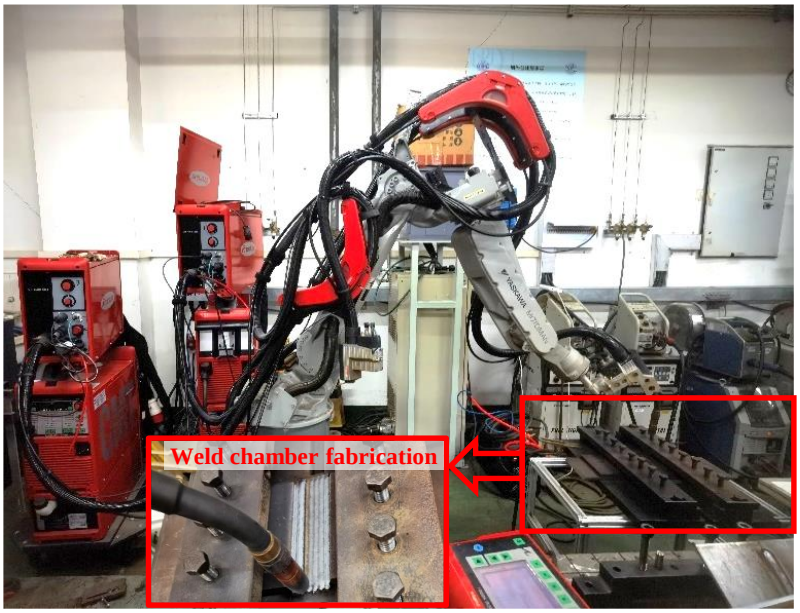

Fig. 2. Welding machine and robotic arm for weld chamber fabrication

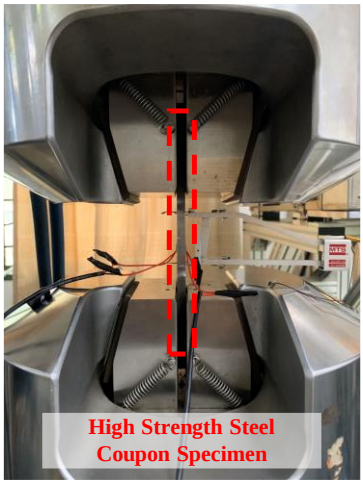

(a) High strength steel coupon tests at ambient temperature

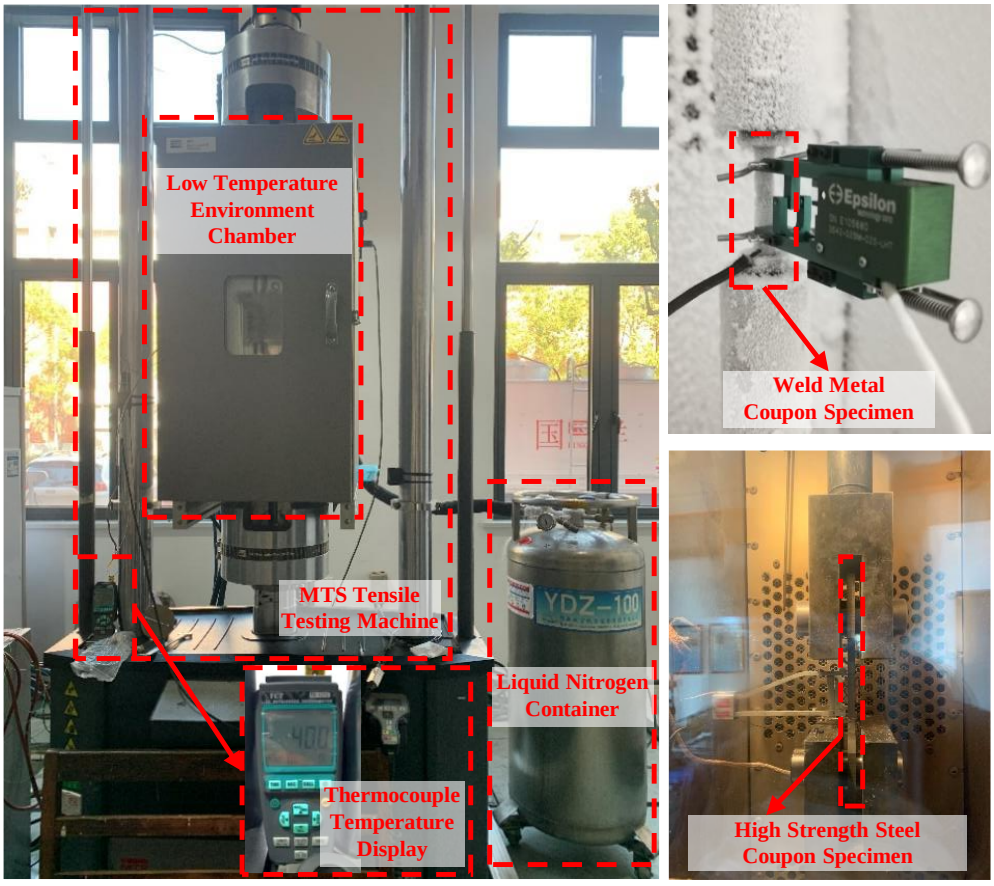

(b) High strength steel and weld metal coupon tests at low temperatures

Fig. 3. Tensile test instrumentations

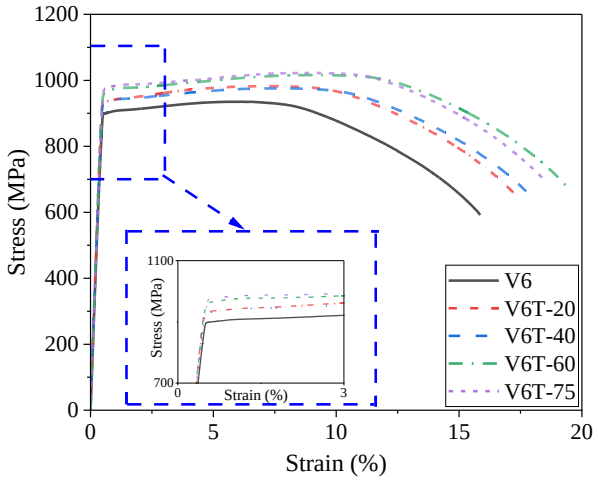

(a) Q890 with t = 6 mm

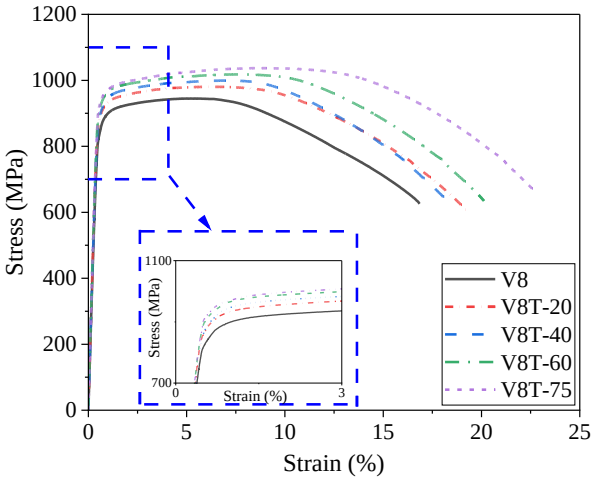

(b) Q890 with t = 8 mm

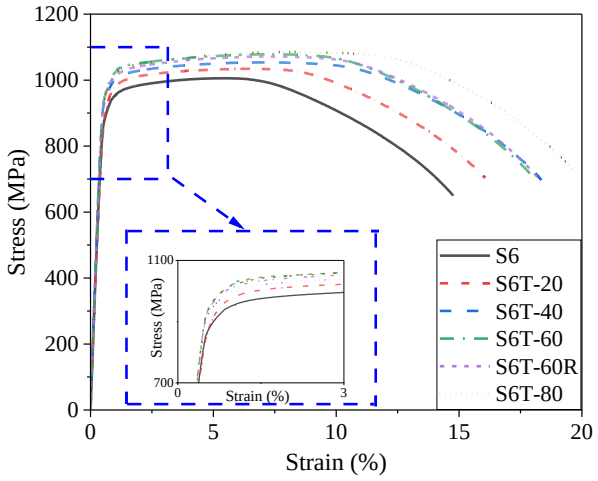

(c) Q960 with t = 6 mm

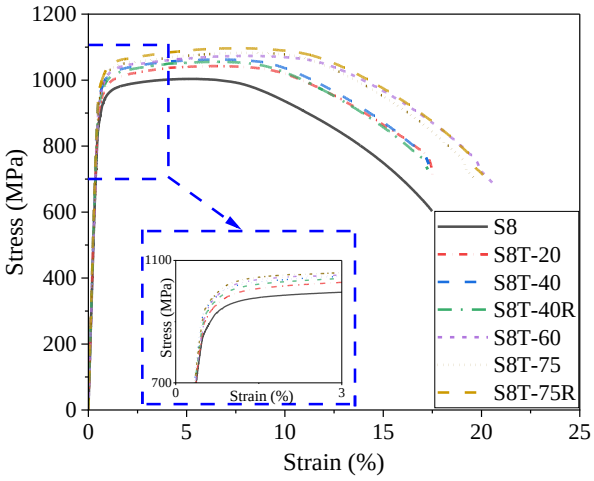

(d) Q960 with t = 8 mm

Fig. 4. Stress-strain responses of high strength steels at ambient and low temperatures

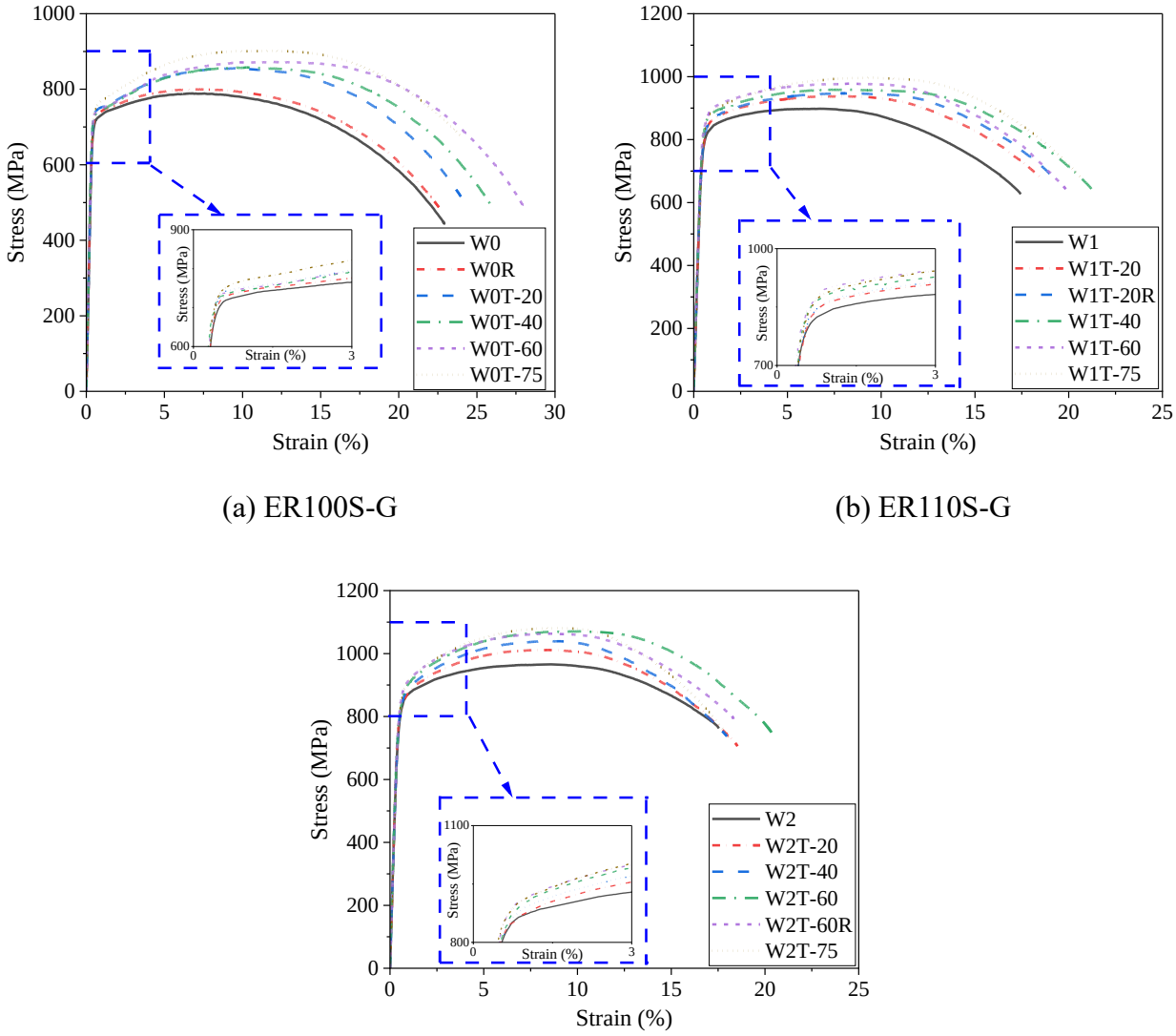

(a) ER100S-G

(b) ER110S-G

(c) ER120S-G

Fig. 5. Stress-strain responses of high strength weld metals at ambient and low temperatures

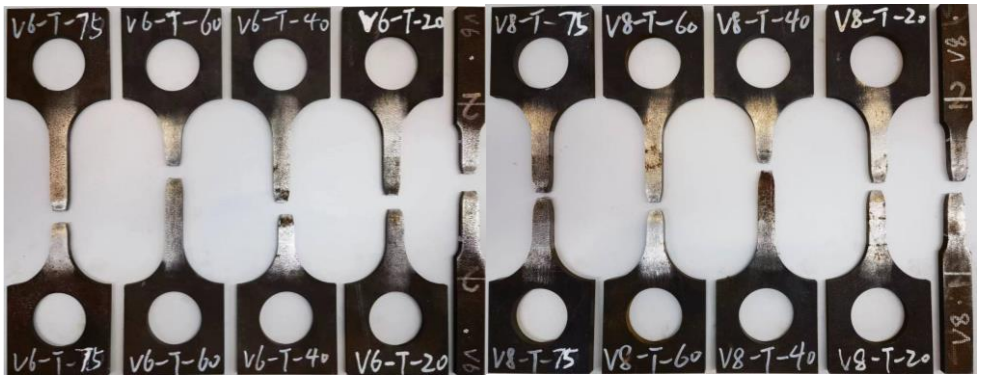

(a) Q890

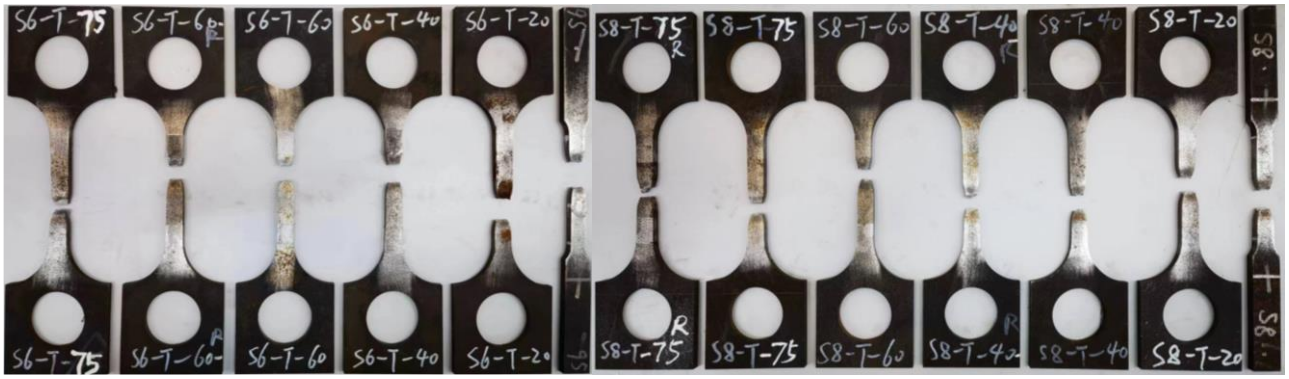

(b) Q960

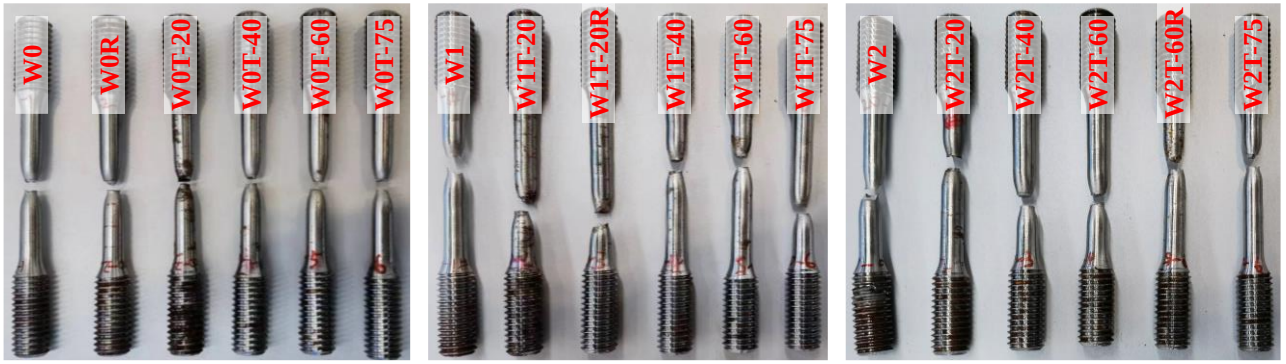

(c) Weld metals

Fig. 6. Tensile coupon specimens after failure at various temperatures

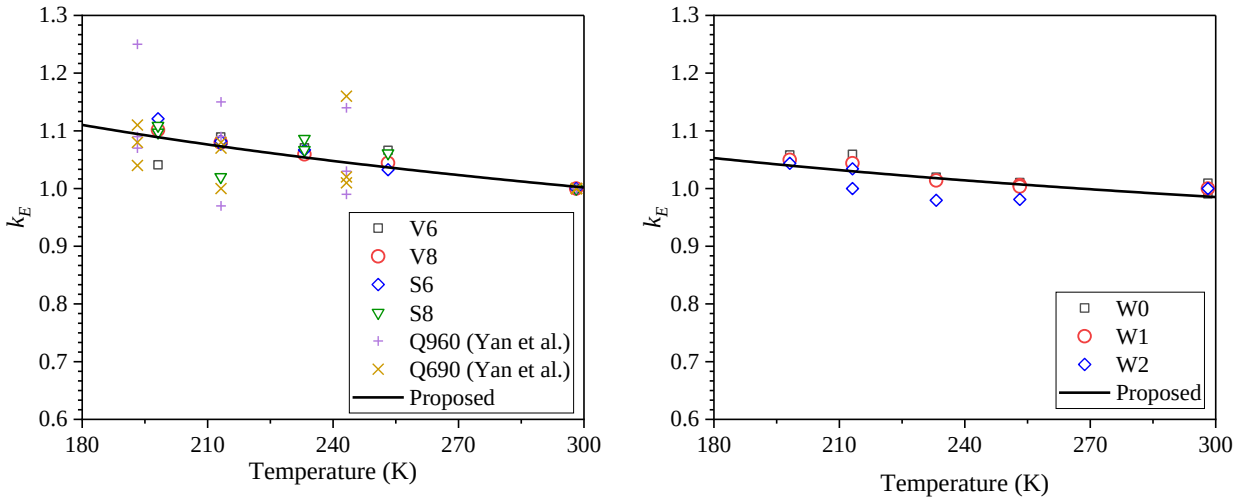

(a) High strength steels (b) Weld metals

Fig. 7. Effect of low temperatures on the Young's modulus

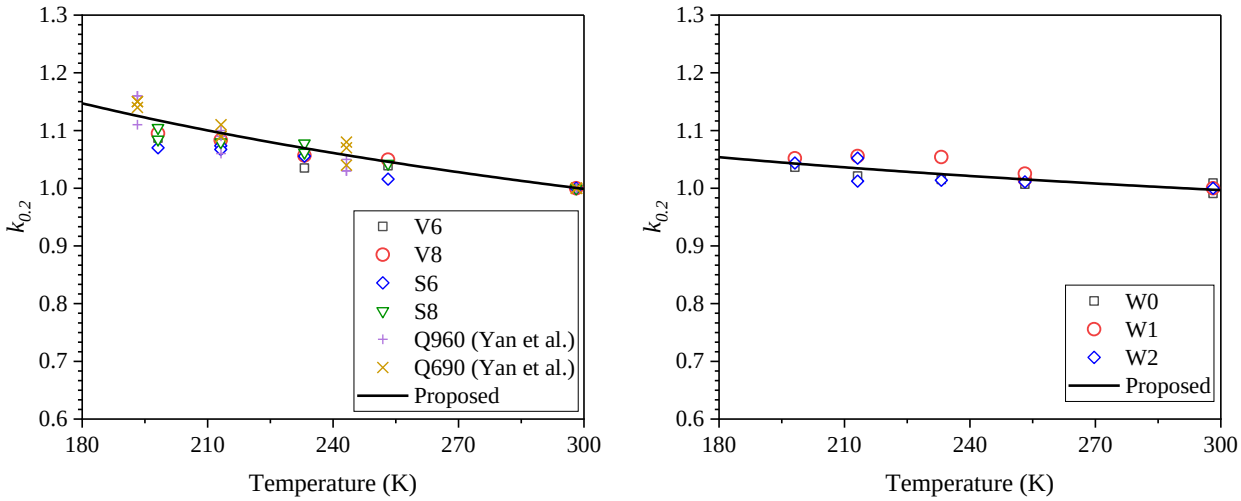

(a) High strength steels (b) Weld metals

Fig. 8. Effect of low temperatures on the yield stress

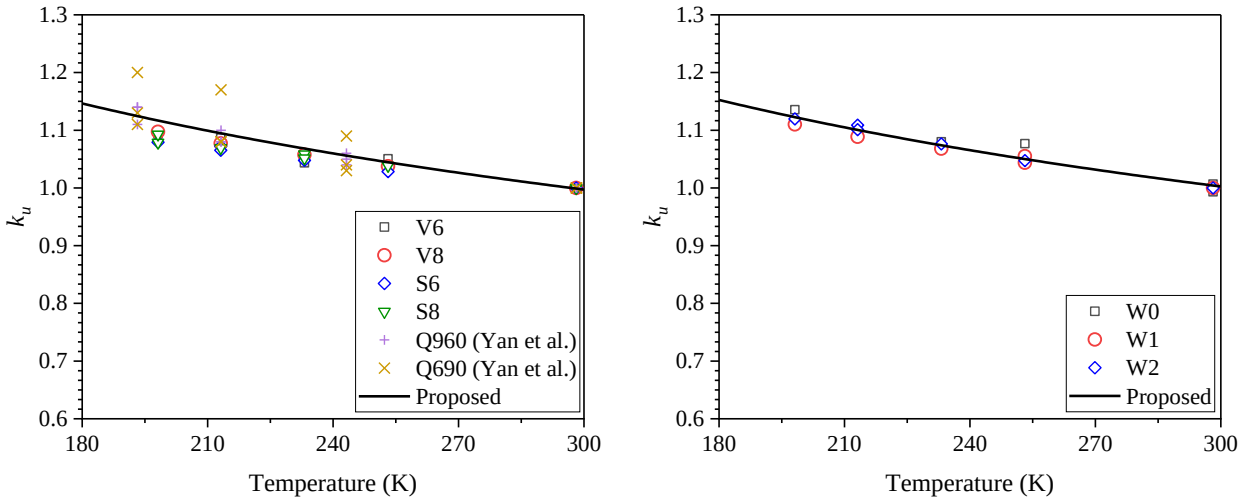

(a) High strength steels (b) Weld metals

Fig. 9. Effect of low temperatures on the ultimate tensile strength

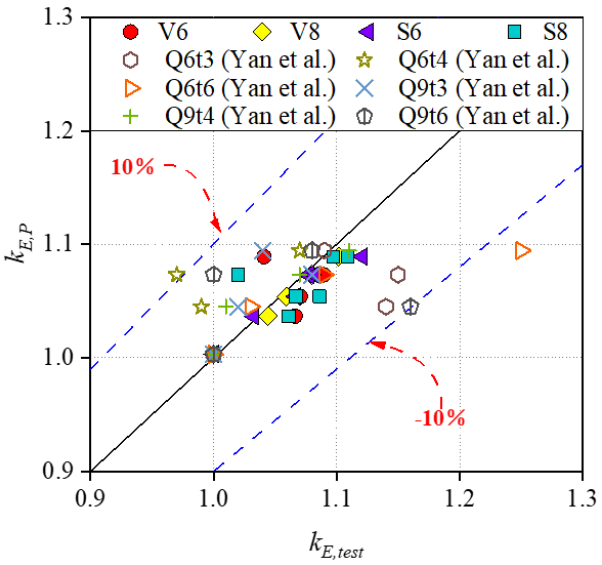

(a) Retention factor of Young's modulus

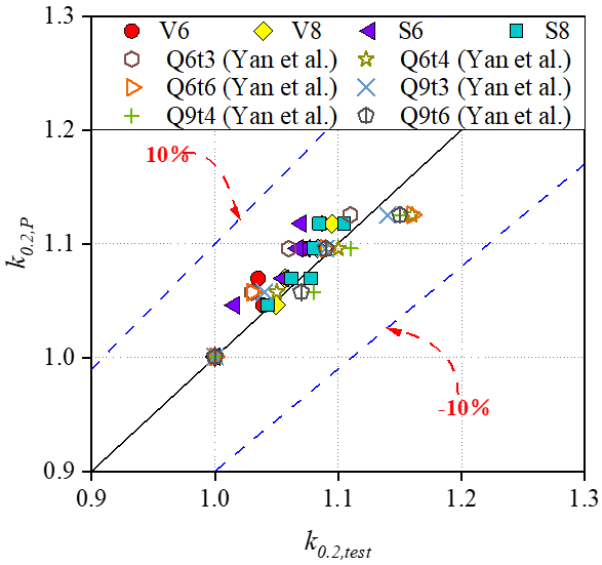

(b) Retention factor of yield stress

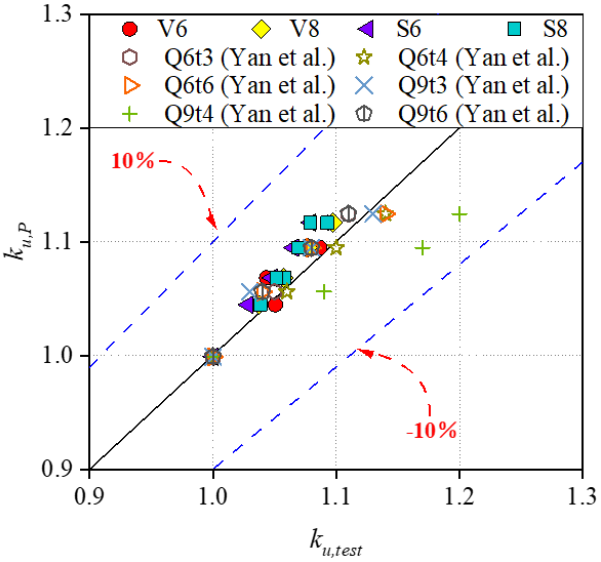

(c) Retention factor of ultimate tensile strength

Fig. 10. Comparisons between test and predicted low temperature retention factors for high strength steels

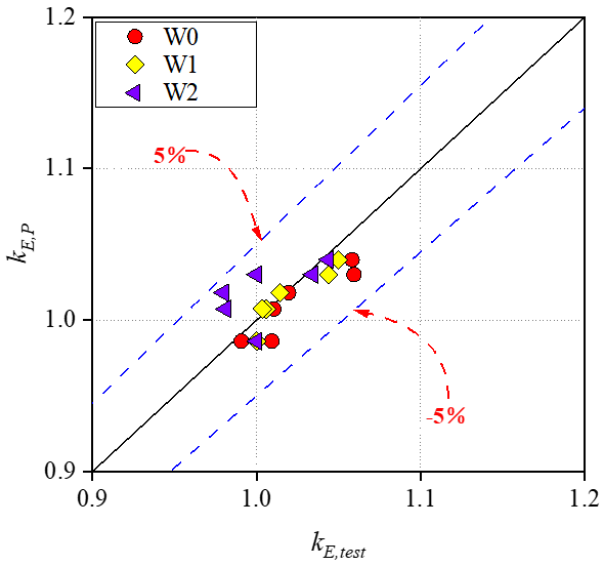

(a) Retention factor of Young's modulus

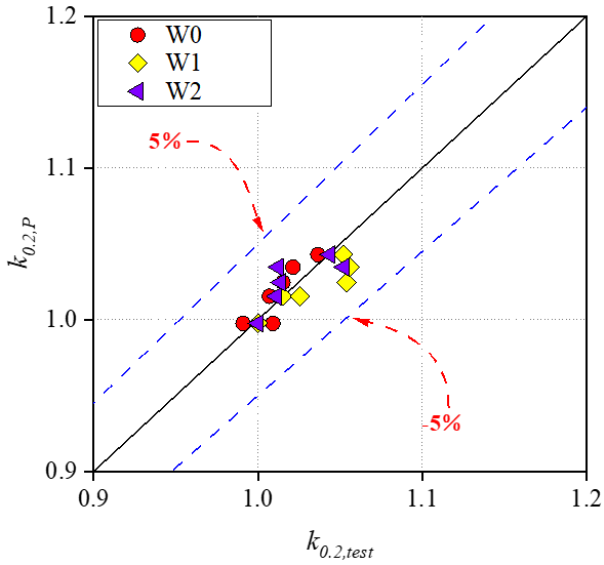

(b) Retention factor of yield stress

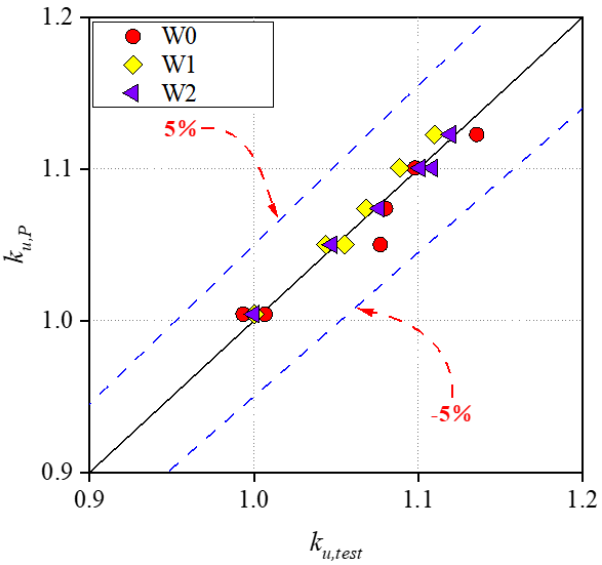

(c) Retention factor of ultimate tensile strength

Fig. 11. Comparisons between test and predicted low temperature retention factors for high strength weld metals

Table 1. Chemical compositions of Q890 and Q960 high strength steels

Steel type	C (%)	Si (%)	Mn (%)	P (%)	S (%)	Cr (%)	Ti (%)	Mo (%)	B (%)	CEV (%)	Ni (%)	Cu (%)	Alt (%)
V6	0.16	0.22	1.19	0.007	0.001	0.25	--	0.465	0.0015	0.51	--	--	--
V8	0.16	0.21	1.17	0.008	0.001	0.24	--	0.460	0.0014	0.51	--	--	--
S6	0.18	0.25	1.02	0.008	0.001	0.34	0.011	0.561	0.0016	0.54	0.04	0.02	0.031
S8	0.17	0.25	1.02	0.008	0.001	0.34	0.015	0.568	0.0015	0.53	0.04	0.03	0.042

Table 2. Measured static material properties of high strength steels and weld metals at ambient temperature

Specimen	E (GPa)	$\sigma_{0.2}$ (MPa)	σ_u (MPa)	ε_f (%)
V6	199.1	900.8	935.2	15.9
V8	198.3	853.7	945.0	16.9
S6	197.7	903.8	1005.8	14.8
S8	198.8	898.5	1003.8	17.5
W0	194.3	714.6	789.0	22.9
W0R	190.7	727.7	799.6	22.6
W1	192.8	803.4	898.3	17.4
W2	201.3	822.7	965.7	17.6

Table 3. Tensile test results and comparisons of high strength steels at arctic low temperatures

Specimen	E_T (GPa)	$\sigma_{0.2T}$ (MPa)	σ_{uT} (MPa)	ε_{fT} (%)	k_E	$k_{0.2}$	k_u	k_f	$E_{T,P}$ (GPa)	$\sigma_{0.2T,P}$ (MPa)	$\sigma_{uT,P}$ (MPa)	$E_T/E_{T,P}$	$\sigma_{0.2T}/\sigma_{0.2T,P}$	$\sigma_{uT}/\sigma_{uT,P}$
V6T-20	212.3	935.9	982.5	17.3	1.07	1.04	1.05	1.09	206.4	942.1	976.8	1.03	0.99	1.01
V6T-40	213.1	932.3	975.9	17.8	1.07	1.04	1.04	1.12	209.9	963.4	999.0	1.02	0.97	0.98
V6T-60	216.9	966.2	1016.2	19.4	1.09	1.07	1.09	1.22	213.7	987.1	1023.8	1.02	0.98	0.99
V6T-75	207.3	978.9	1022.5	18.4	1.04	1.09	1.09	1.16	216.8	1006.8	1044.4	0.96	0.97	0.98
V8T-20	207.0	896.0	980.6	19.3	1.04	1.05	1.04	1.14	205.5	892.8	987.1	1.01	1.00	0.99
V8T-40	210.0	902.1	999.3	18.5	1.06	1.06	1.06	1.10	209.0	913.0	1009.6	1.00	0.99	0.99
V8T-60	214.0	924.8	1018.1	20.1	1.08	1.08	1.08	1.19	212.8	935.4	1034.6	1.01	0.99	0.98
V8T-75	218.4	934.7	1037.0	22.8	1.10	1.09	1.10	1.35	215.9	954.1	1055.4	1.01	0.98	0.98
S6T-20	204.1	918.0	1034.3	16.1	1.03	1.02	1.03	1.09	204.9	945.2	1050.6	1.00	0.97	0.98
S6T-40	210.8	953.9	1053.8	18.4	1.07	1.06	1.05	1.24	208.3	966.6	1074.4	1.01	0.99	0.98
S6T-60	212.9	970.2	1078.4	18.1	1.08	1.07	1.07	1.22	212.1	990.3	1101.1	1.00	0.98	0.98
S6T-60R	213.9	964.5	1071.5	18.2	1.08	1.07	1.07	1.23	212.1	990.3	1101.1	1.01	0.97	0.97
S6T-75	221.6	967.1	1085.5	19.6	1.12	1.07	1.08	1.33	215.3	1010.1	1123.2	1.03	0.96	0.97
S8T-20	211.0	936.7	1042.4	17.5	1.06	1.04	1.04	1.00	206.1	939.7	1048.5	1.02	1.00	0.99
S8T-40	216.0	968.5	1062.3	17.3	1.09	1.08	1.06	0.99	209.6	960.9	1072.3	1.03	1.01	0.99
S8T-40R	212.2	954.0	1055.5	17.3	1.07	1.06	1.05	0.99	209.6	960.9	1072.3	1.01	0.99	0.98
S8T-60	202.8	970.2	1073.4	20.8	1.02	1.08	1.07	1.19	213.4	984.5	1098.9	0.95	0.99	0.98
S8T-75	218.2	974.4	1082.9	19.6	1.10	1.08	1.08	1.12	216.5	1004.2	1121.0	1.01	0.97	0.97
S8T-75R	220.5	992.6	1096.9	20.3	1.11	1.10	1.09	1.16	216.5	1004.2	1121.0	1.02	0.99	0.98
Q6t3T-30*	229.0	688.0	782.0	--	1.14	1.03	1.05	--	210.7	706.5	784.5	1.09	0.97	1.00
Q6t3T-60*	231.0	705.5	799.5	--	1.15	1.06	1.08	--	216.3	732.2	813.2	1.07	0.96	0.98
Q6t3T-80*	219.0	739.0	824.0	--	1.09	1.11	1.11	--	220.6	752.0	835.4	0.99	0.98	0.99
Q6t4T-30*	191.0	720.0	811.0	--	1.14	1.03	1.05	--	202.4	728.1	806.8	0.94	0.99	1.01
Q6t4T-60*	187.5	755.0	839.0	--	1.15	1.06	1.08	--	207.8	754.5	836.4	0.90	1.00	1.00
Q6t4T-80*	207.5	796.5	871.0	--	1.09	1.11	1.11	--	211.9	774.9	859.2	0.98	1.03	1.01
Q6t6T-30*	186.0	664.0	755.0	--	0.99	1.05	1.06	--	189.5	679.6	768.2	0.98	0.98	0.98
Q6t6T-60*	198.0	697.5	784.5	--	0.97	1.10	1.10	--	194.6	704.3	796.4	1.02	0.99	0.99
Q6t6T-80*	226.0	743.0	832.0	--	1.07	1.16	1.14	--	198.5	723.3	818.1	1.14	1.03	1.02
Q9t3T-30*	201.0	1007.0	1043.0	--	1.03	1.03	1.04	--	206.5	1027.8	1073.9	0.97	0.98	0.97
Q9t3T-60*	212.5	1064.0	1097.0	--	1.09	1.09	1.08	--	212.0	1065.1	1113.2	1.00	1.00	0.99
Q9t3T-80*	205.0	1109.0	1148.0	--	1.25	1.16	1.14	--	216.3	1094.0	1143.6	0.95	1.01	1.00
Q9t4T-30*	196.0	1009.5	1033.0	--	1.02	1.04	1.03	--	202.9	990.7	1004.5	0.97	1.02	1.03
Q9t4T-60*	208.0	1038.0	1113.5	--	1.08	1.09	1.08	--	208.3	1026.7	1041.3	1.00	1.01	1.07
Q9t4T-80*	216.0	1078.5	1138.5	--	1.04	1.14	1.13	--	212.5	1054.5	1069.7	1.02	1.02	1.06
Q9t6T-30*	213.0	974.0	1029.0	--	1.01	1.08	1.09	--	191.5	962.9	1043.3	1.11	1.01	0.99
Q9t6T-60*	183.0	994.0	1062.0	--	1.07	1.11	1.17	--	196.6	997.9	1081.5	0.93	1.00	0.98
Q9t6T-80*	198.0	1050.0	1094.0	--	1.11	1.15	1.20	--	200.5	1024.9	1111.0	0.99	1.02	0.98
											Mean	1.005	0.992	0.992
											COV	0.046	0.019	0.023

Note: * marks the test specimens reported in Yan *et al.* [74]

Table 4. Tensile test results and comparisons of high strength weld metals at arctic low temperatures

Specimen	E_T (GPa)	$\sigma_{0.2T}$ (MPa)	σ_{uT} (MPa)	ε_{fT} (%)	k_E	$k_{0.2}$	k_u	k_f	$E_{T,P}$ (GPa)	$\sigma_{0.2T,P}$ (MPa)	$\sigma_{uT,P}$ (MPa)	$E_T/E_{T,P}$	$\sigma_{0.2T}/\sigma_{0.2T,P}$	$\sigma_{uT}/\sigma_{uT,P}$
W0T-20	194.5	726.1	855.3	24.0	1.01	1.01	1.08	1.05	193.9	732.2	834.0	1.00	0.99	1.03
W0T-40	196.3	732.1	857.8	26.0	1.02	1.02	1.08	1.13	196.0	738.8	853.0	1.00	0.99	1.01
W0T-60	203.9	736.4	872.1	28.0	1.06	1.02	1.10	1.22	198.3	746.1	874.1	1.03	0.99	1.00
W0T-75	203.7	747.4	902.0	24.0	1.06	1.04	1.14	1.04	200.2	752.0	891.7	1.02	0.99	1.01
W1T-20	193.9	815.5	937.5	18.6	1.01	1.02	1.04	1.07	194.2	815.7	943.2	1.00	1.00	0.99
W1T-20R	193.5	823.8	947.7	19.0	1.00	1.03	1.06	1.09	194.2	815.7	943.2	1.00	1.01	1.00
W1T-40	195.5	846.8	959.4	21.4	1.01	1.05	1.07	1.23	196.3	823.1	964.6	1.00	1.03	0.99
W1T-60	201.3	848.2	977.9	19.8	1.04	1.06	1.09	1.14	198.6	831.2	988.6	1.01	1.02	0.99
W1T-75	202.4	845.0	997.0	20.8	1.05	1.05	1.11	1.19	200.5	837.8	1008.4	1.01	1.01	0.99
W2T-20	197.5	831.8	1011.5	18.5	0.98	1.01	1.05	1.05	202.7	835.3	1014.0	0.97	1.00	1.00
W2T-40	197.2	834.0	1039.4	18.0	0.98	1.01	1.08	1.02	204.9	842.8	1037.1	0.96	0.99	1.00
W2T-60	208.2	832.8	1070.7	20.4	1.03	1.01	1.11	1.16	207.3	851.1	1062.8	1.00	0.98	1.01
W2T-60R	201.3	865.7	1063.3	18.3	1.00	1.05	1.10	1.04	207.3	851.1	1062.8	0.97	1.02	1.00
W2T-75	210.1	858.6	1081.1	18.1	1.04	1.04	1.12	1.03	209.3	857.9	1084.2	1.00	1.00	1.00
											Mean	0.999	1.001	1.001
											COV	0.018	0.014	0.010

Table 5. Results of the best subset regression analyses for high strength steel

Mechanical property	Model No.	Predictors	R^2	Cp	*a*	*b*	*c*
E_T	1	*T*	0.27	1.09	3.153	-0.201	--
	2	*E*	0.00	21.23	0.933	--	0.023
	3	*T, E*	0.27	3.00	2.326	-0.202	0.058
$\sigma_{0.2T}$	1	*T*	0.81	1.45	4.686	-0.271	--
	2	$\sigma_{0.2}$	0.00	235.27	1.044	--	0.003
	3	*T,* $\sigma_{0.2}$	0.81	3.00	4.338	-0.272	0.012
σ_{uT}	1	*T*	0.74	1.39	4.732	-0.273	--
	2	σ_u	0.01	158.45	1.291	--	-0.028
	3	*T,* σ_u	0.75	3.00	5.243	-0.273	-0.016

Table 6. Results of the best subset regression analyses for high strength weld metal

Mechanical property	Model No.	Predictors	R^2	Cp	*a*	*b*	*c*
E_T	1	*T*	0.54	0.43	2.068	-0.130	--
	2	*E*	0.14	-0.15	14.596	--	-0.504
	3	*T, E*	0.69	0.46	29.640	-0.130	-0.504
$\sigma_{0.2T}$	1	*T*	0.66	3.37	1.856	-0.109	--
	2	$\sigma_{0.2}$	0.06	29.32	0.610	--	0.078
	3	*T,* $\sigma_{0.2}$	0.72	3.00	1.105	-0.109	0.078
σ_{uT}	1	*T*	0.95	3.91	4.757	-0.273	--
	2	σ_u	0.01	288.62	11.467	--	-0.047
	3	*T,* σ_u	0.96	3.00	1.876	-0.273	-0.047